Available online at www.sciencedirect.com
SCIENCE DIRECT
Biochemical Pharmacology 68 (2004) 2387–2396
Biochemical Pharmacology
www.elsevier.com/locate/biochempharm

Involvement of both endoplasmic reticulum and mitochondria in photokilling of nasopharyngeal carcinoma cells by the photosensitizer Zn–BC–AM

Nai-Ki Mak[a,*], Kai-Man Li[a], Wing-Nang Leung[b], Ricky Ngok-Shun Wong[a], Dolly P Huang[c], Maria Li Lung[d], Yan-Kin Lau[e], Chi K Chang[e]

[a]*Department of Biology, Hong Kong Baptist University, Hong Kong, China*
[b]*School of Chinese Medicine, Hong Kong Baptist University, Hong Kong, China*
[c]*Department of Anatomical and Cellular Pathology, Chinese University of Hong Kong, Hong Kong, China*
[d]*Department of Biology, Hong Kong University of Science and Technology, Hong Kong, China*
[e]*Department of Chemistry, Hong Kong University of Science and Technology, Hong Kong, China*

Received 11 March 2004; accepted 20 August 2004

Abstract

Photodynamic therapy (PDT) is recently developed as an effective treatment for malignant disease. In PDT, the photosensitizer eradicates tumour by induction of apoptosis. In this study, we investigated the mechanistic actions of a recently developed second generation photosensitizer, Zn–BC–AM, on nasopharyngeal carcinoma (NPC) cells. Zn–BC–AM was found to localize in the mitochondria, endoplasmic reticulum (ER), and golgi body. Photoactivation of Zn–BC–AM loaded NPC cells resulted in a rapid collapse of mitochondrial membrane potential ($\Delta\psi_m$) (15 min), followed by the release of cytochrome *c* (1 h), and activation of caspases-9 and -3 (4 h). Expression of ER chaperones Bip/Grp78 and Grp94, and ER resident lectin-like chaperone calnexin (CNX) was also enhanced in PDT-stressed NPC cells. Caspase-12, an important caspase involved in ER stress-induced apoptosis, was also activated. Inhibition of Ca^{2+} uptake into mitochondria by ruthenium red (RR) or loading the cells with EGTA–AM, an agent that buffers intracellular Ca^{2+} released from ER, resulted in a significant reduction of Zn–BC–AM PDT-induced cell death. These observations suggest that both ER and mitochondria are the subcellular targets of Zn–BC–AM. Effective activation of ER- and mitochondria-mediated apoptotic pathways is responsible for Zn–BC–AM PDT-induced NPC cell death.

Keywords: Nasopharyngeal carcinoma; Photodynamic therapy; ER-stress; Mitochondrial membrane potential; Caspase-12

1. Introduction

Nasopharyngeal carcinoma (NPC) is one of the major causes of death in Hong Kong and Southern China. The disease is rare in Europe and North America, and very few oncologists in the Western world have extensive experience in treating this neoplasm [1]. NPC is a malignant squamous cell carcinoma and radiotherapy is the primary form of treatment. The combination of radiotherapy and chemotherapy are used for the treatment of advanced stage NPC. Photodynamic therapy (PDT) is a cancer treatment modality applicable for a wide variety of tumours. These include the use of ALA for skin cancer [2] and porfimer sodium (Photofrin) for endobronchial and oesophageal tumours [3]. PDT involves the sensitization of tumour cells with a photosensitizing compound followed by exposure of the sensitized tissue to visible light [4]. Photoactivation of the sensitizer results in the liberation of highly reactive oxygen species and cell death. Both necrotic and apoptotic cell death have been reported in PDT-induced tumour cell death [5]. Among those recently developed photosensitizers, long-wavelength-absorbing photosensitizers, such as benzochlorins received much interest. Zn(II) benzochlorin analog was found to be quite effective in tumour eradication in vivo [6].

Earlier studies showed the unique subcellular localization of PDT compounds. Cationic photosensitizer triaryl

Abbreviations: $\Delta\psi_m$, mitochondrial membrane potential; CNX, calnexin; ER, endoplasmic reticulum; NPC, nasopharyngeal carcinoma; PDT, photodynamic therapy; ROS, reactive oxygen species; RR, ruthenium red

* Corresponding author. Tel.: +852 3411 7059; fax: +852 3411 5995.
E-mail address: nkmak@hkbu.edu.hk (N.-K. Mak).

0006-2952/$ – see front matter © 2004 Elsevier Inc. All rights reserved.
doi:10.1016/j.bcp.2004.08.024

methane dye Victoria Blue BO (VBBO) was found to localize in mitochondria [7]. In human epidermoid carcinoma A431 cells, the plasma membranes and golgi complex were the main target sites of photofrin [8]. The initial oxidative reactions lead to damage to organelles in which the dye is bound, culminating in cell death and destruction of the tumour or abnormal tissue [9]. Both the plasma membrane [8] and mitochondria [10] have been implicated in PDT-induced apoptotic cell death.

Several distinct apoptotic pathways have recently been established [11]. These include the ligand binding of death receptor expressed on the tumour cell surface, oxidative stress on the mitochondria, and the induction of ER stress. Other intracellular signaling pathways have also been implicated in modulating PDT-induced tumour cell death. PDT-induced tumour cell apoptosis was increased by blocking the p38MAP kinase cascade pathway [12]. In this study, the induction of ER stress during photodynamic treatment of nasopharyngeal carcinoma cells (NPC) was investigated. We herein show the subcellular localization of a Zn(II) benzochlorin analog Zn–BC–AM and the involvement of both mitochondria and ER in apoptosis of the NPC cells.

2. Materials and methods

2.1. NPC cell lines and chemicals

In Hong Kong, most of the nasopharyngeal carcinomas are undifferentiated carcinomas or poorly differentiated squamous cell carcinomas. In this study, poorly differentiated CNE-2 and undifferentiated HONE-1 squamous cell carcinoma cell lines were grown in 10% heat-inactivated fetal calf serum (FCS, Gibco), 2 mM glutamine, and antibiotics (50 μg/ml penicillin and 50 μg/ml streptomycin, Gibco) supplemented RPMI-1640 and DMEM medium, respectively. Ruthenium red (RR) was obtained from Calbiochem.

2.2. Synthesis of photosensitizer Zn–BC–AM

The synthetic scheme of Zn–BC–AM (**5**) is shown in Fig. 1. To 2,3,8,8,12,13,17,18-octaethylbenzochlorin (100 mg) in a V-vial (1 ml) reaction tube under nitrogen was added 750 μl thionyl bromide by micro-syringe. The resulting solution was stirred for 2 h under nitrogen. The solution was then transferred into a separatory funnel and 20 ml dichloromethane was added, followed by 20 ml of saturated sodium bicarbonate solution. The organic layer was separated and the aqueous layer was extracted three times with 10 ml dichloromethane. The combined organic layer was washed by 20 ml water and then dried by anhydrous magnesium sulfate. The solvent was removed under vacuum and the resulting residue was chromatographed on silica gel with hexane-dichloromethane (1:1) as eluent. The desired green band was collected and crystallized from dichloromethane and methanol to give (**1**) (73 mg, 64%). UV–vis: λ 411, 532, 564, 605 and 655 nm; ^{1}H NMR (300 MHz, $CDCl_3$) δ 0.14–0.18 (6H, t, *gem* CH_3), 1.29–1.74 (18H, overlapping t, CH_3 of peripheral methyl), 2.57

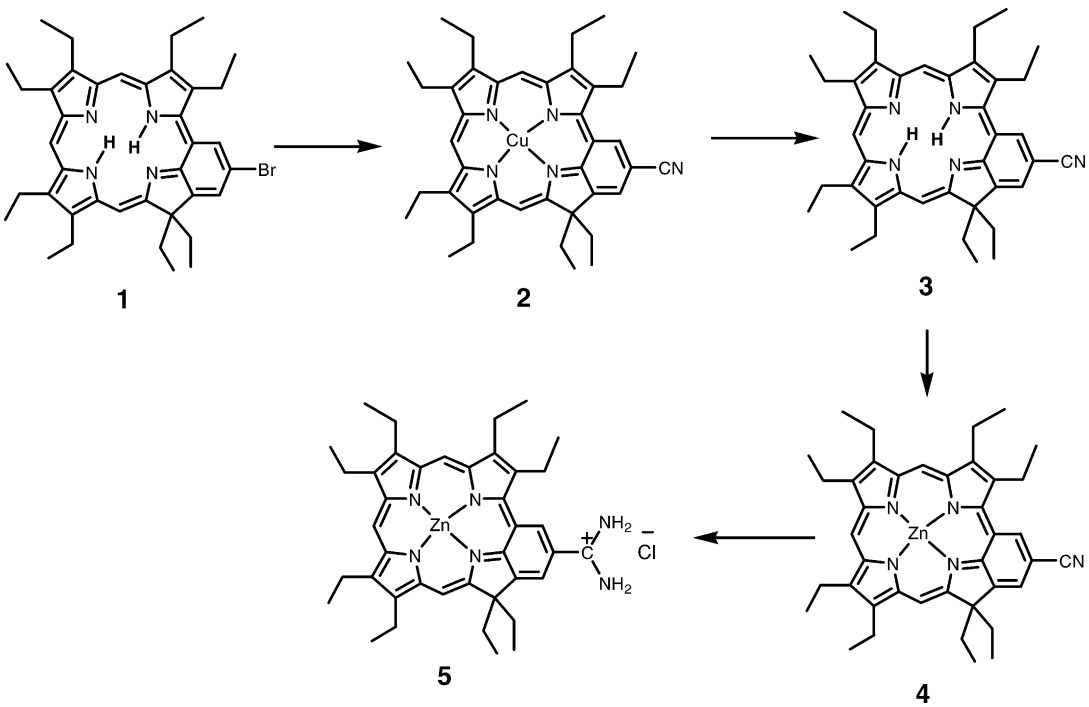

Fig. 1. Synthetic scheme of Zn–BC–AM (**5**). 5^{2-}Bromo-2,3,8,8,12,13,17,18-octaethyl-benzochlorin (**1**), copper(II) 5^2-cyano-2,3,8,8,12,13,17,18-octaethyl-benzochlorin (**2**), 5^2-cyano-2,3,8,8,12,13,17,18-octaethylbenzochlorin (**3**), zinc (II) 5^2-cyano-2,3,8,8,12,13,17,18-octaethylbenzochlorin (**4**), zinc (II) 2,3,8,8,12,13,17,18-octaethylbenzochlorin amidinium salt (**5**).

(4H, overlapping q, *gem* CH_2), 3.52–3.93 (12H, overlapping q, CH_2 of peripheral ethyl), 7.99, 8.59 and 9.23 (1H each, s, *meso* H 8.08, 9.65 (1H each, s, H of benzene ring); MS found *m/e* 652.4; calculated 651.7 for $C_{39}H_{47}N_4Br$.

2.3. Copper(II) 5^2-cyano-2,3,8,8,12,13,17, 18-octaethylbenzochlorin (**2**)

Copper(II) cyanide (30 mg) was added to a solution of 50 mg of (**1**) in 30 ml dimethylformamide and the mixture was refluxed for 24 h. The solution was washed by 100 ml water twice and extracted by dichloromethane. The resulting organic layer was dried by anhydrous magnesium sulfate and solvent was removed under reduced pressure. Purification was done by chromatography with hexane-dichloromethane (1:9) as eluent to give the desired compound in 88% yield. UV–vis: λ 416, 532, 564, 617 and 660 nm; MS found *m/e* 661.0; calculated 661.4 for $C_{40}H_{45}N_5Cu$.

2.4. 5^2-Cyano-2,3,8,8,12,13,17,18-octaethylbenzochlorin (**3**)

Concentrated sulfuric acid (5 ml) was added to a solution of 50 mg of (**2**) in 20 ml dichloromethane and stirred until all the green color concentrated into the acid layer (ca. 20 min). Ice and saturated sodium hydrogen carbonate solution was added to neutralize the acid. The product was extracted by dichloromethane. The resulting organic layer was dried by anhydrous magnesium sulfate and solvent was removed under reduced pressure. Purification was done by chromatography with hexane-dichloromethane (6:4) as eluent to give the desired compound (**3**) in 88% yield. UV–vis: λ 413, 529, 562, 615 and 657 nm; ^{1}H NMR (300MHz, $CDCl_3$) δ 0.01–0.06 (6H, t, *gem* CH_3), 1.62–1.74 (18H, overlapping t, CH_3 of peripheral methyl), 2.56–2.73 (4H, overlapping q, *gem* CH_2), 3.49–3.93 (12H, overlapping q, CH_2 of peripheral ethyl), 8.06, 8.68, 9.29 (1H each, s, *meso* H), 8.19, 9.93 (1H each, s, H of benzene ring); MS found *m/e* 597.4; calculated 597.8 for $C_{40}H_{47}N_5$.

2.5. Zinc(II) 5^2-cyano-2,3,8,8,12,13,17, 18-octaethylbenzochlorin (**4**)

Zinc(II) acetate (70 mg) dissolved in 20 ml methanol was added to a solution of 50 mg of (**3**) in 30 ml chloroform. The mixture was refluxed until chelation was complete (monitored by both UV–vis and TLC, ca. 30 min). The mixture was added to water and followed by dichloromethane. The organic layer was washed twice with water. After removal of solvent, the solid residue was chromatographed on silica gel using methanol/dichloromethane (1:9) as eluent to give the product in 84% yield. UV–vis: λ 427, 523, 565, 623 and 677 nm; ^{1}H NMR (300 MHz, $CDCl_3$) δ 0.06–0.11 (6H, t, *gem* CH_3), 1.65–1.73 (18H, overlapping t, CH_3 of peripheral methyl), 2.55–2.68 (4H, overlapping q, *gem* CH_2), 3.52–3.89 (12H, overlapping q, CH_2 of peripheral ethyl), 8.07, 8.89 and 9.33 (1H each, s, *meso* H), δ 8.16 and 10.02 (1H each, s, H of benzene ring); MS found *m/e* 659.3; calculated 661.2 for $C_{40}H_{45}N_5Zn$.

2.6. Zinc(II) 2,3,8,8,12,13,17,18-octaethylbenzochlorin amidinium salt (**5**)

To a Schlenk tube, 35 mg of (**4**) and 20 ml dried toluene was added. After the system was purged with nitrogen three times, 1 ml of 1 M methyl aluminium(III) chloroamide was introduced by syringe. The reaction mixture was stirred at 80 °C for 48 h under nitrogen. Thirty-millilitre dichloromethane was added after the mixture had been stirred in the air for 2 more hours. Precipitates in the mixture were filtered off and the filtrate was dried under reduced pressure. The solid residue was chromatographed on silica gel using methanol/dichloromethane (15:85) as eluent to give 57% yield. UV–vis: λ 452, 550, 603, 642 and 700 nm; ^{1}H NMR (300 MHz, $CDCl_3$) δ 0.14–0.10 (6H, t, *gem* CH_3), 1.65–1.77 (18H, overlapping t, CH_3 of peripheral methyl), 2.43 (4H, overlapping q, *gem* CH_2), 3.49–3.71 (12H, overlapping q, CH_2 of peripheral ethyl), 7.91, 8.84 and 9.39 (1H each, s, *meso* H), 8.28, 10.02 (1H each, s, H of benzene ring); 8.70 (NH, board) MS found *m/e* 730.1; calculated 732.6 for $C_{40}H_{49}N_6Sn$. The purity of Zn–BC–AM used in this study was 99.2%.

2.7. Cytotoxicity assay

MTT (3-(4,5-dimethylthiazol-2-yl)-2,5 diphenyl-tetrazolium bromide) reduction assay was used to measure the photocytotoxicity of Zn–BC–AM on the NPC cells [13]. Briefly, NPC cells (1×10^4 cells/well) in 96-well flat-bottomed tissue culture plates were incubated with various concentrations of Zn–BC–AM (0–2 μM) for 24 h at 37 °C. Cells were then exposed to light emitted from a 400-watt tungsten lamp with a heat isolation filter and 682 ± 5 nm narrow band filter at an intensity of 7 mW/cm^2. Cells were then incubated at 37 °C in a CO_2 incubator for 24 h. The optical density (OD) of the dissolved formazan crystals was measured using an IEMS Analyzer (Lab-system, Type 1401) at wavelengths of 570 and 690 nm. The percentage of cytotoxicity was calculated using the following equation: cytotoxicity (%) = $(OD_{\text{control group}} - OD_{\text{treatment group}})/OD_{\text{control group}} \times 100$, where $OD = OD_{570-690\ \text{nm}}$.

2.8. Flow cytometric analysis

Overnight cultured NPC cells (1×10^5 cells) were treated with the sensitizers for 1–24 h in wells of six-well plates. The cells were trypsinized and washed with PBS to remove the sensitizers. The cells were then fixed with paraformaldehyde (3% in PBS), and the fluorescence profiles of stained cells were analyzed using FACSCalibur

(Becton Dickinson). The laser line with a wavelength of 488 nm was used for excitation, and the fluorescence signal was detected using the FL-3 channel (long pass filter 670 nm). At least 10,000 events were counted.

2.9. Confocal microscopy

A laser scanning confocal microscope (Zeiss LSM 510) with epifluorescence and a phase contrast system was used to study the subcellular localization of Zn–BC–AM [14]. An argon/krypton laser line with a wavelength of 488 nm was used for the excitation of organelle probes and the He–Ne laser line was used for the excitation of Zn–BC–AM. The band pass filter (BP 505–550 nm) and long pass filter (LP 650 nm) were used at the emission end for the detection of the organelle probes and the sensitizers, respectively. The pinhole size of 120 μm was selected to exclude fluorescence light emitted from out-of-focus planes above and below the focusing plane. A water immersion objective with magnification of 63 times was used for image capturing. The images were analyzed using the latest software LSM510 Release 2.01.

2.10. Mitochondrial membrane potential

The change of mitochondrial membrane potential ($\Delta\psi_m$) was monitored using the flow cytometric method [15]. Briefly, CNE-2 cells were treated with the sensitizers (2 μM) for 24 h. The cells were then irradiated at the light dose of 5 J/cm^2 and further incubated for 15–60 min. The voltage-sensitive dye tetramethylrhodamine ethyl ester (TMRE, 150 nM) was then added 30 min before cell harvesting. The washed cells were resuspended in FACS buffer (PBS containing 1% BSA, 0.01% sodium azide and 15 nM TMRE). The cells were analyzed using a FACS-Calibur (Becton Dickson) with the excitation setting at 488 nm and the signals were acquired at the FL-2 channel. Data were analyzed using the CellQuest software.

2.11. Western blotting

Zn–BC–AM PDT treated CNE-2 cells were harvested and the expression of caspase-12 and the stress-induced molecular chaperone Grp94 and Grp78 in Zn–BC–AM PDT treated CNE-2 cells was analyzed using the Western blotting technique. After PDT, the cells were washed with PBS and then lysed with lysis buffer (250 mM Tris–HCl, pH 8, 1% NP-40 and 150 mM NaCl). The cell lysate containing 100 μg of total cellular protein was subjected to electrophoresis in 10% SDS-PAGE. The separated proteins were electrophoretically blotted onto Immuno-Blot PVDF™ membrane (Bio-Rad). Both electrophoresis and blotting were performed using the Mini-PROTEAN® 3 electrophoresis system (Bio-Rad). Western blot was conducted using the ECL™ Western Blotting Detection Reagents (Amersham Biosciences, RPN2209). The primary antibodies were rabbit anti-caspase-12 (Ab-1 and Ab-2) from Oncogene, anti-calnexin (SPA-860, Stressgen), and anti-KDEL (SPA-827, Stressgen, Canada). Caspase-12 Ab-1 and Ab-2 were raised against the synthetic peptide corresponding to amino acids 100–116 and 2–17 of murine caspase-12, respectively. These antibodies have been shown to react with human caspase-12. The anti-KDEL monoclonal was raised against the synthetic peptide SEKDEL based on the rat Grp78 (amino acids 649–654). This antibody identifies the Grp78 (Bip) and Grp94.

3. Results

3.1. Synthesis and absorption characteristics of Zn–BC–AM

When 2,3,8,8,12,13,17,18-octaethylbenzochlorin was treated with thionyl bromide, followed by firstly a substitution reaction with copper(II) cyanide and then zinc metal replacement, of the desired cyano precursor (**4**) could be obtained with an overall yield of about 42% from the starting material. The Zn–BC–AM (**5**) was then synthesized from the cyano compound by reacting (**4**) with methyl aluminium(III) chloroamide. The yield of this last step was 57%. During PDT, photosensitizers are activated by light of a sufficiently long wavelength for tissue penetration. The visible absorption spectrum of Zn–BC–AM was then measured in dichloromethane showing the prominent absorption band in the 680 nm region (Fig. 2). Compared to the unsubstituted benzochlorin, introduction of the amidinium group produced a significant bathochromic shift in the long wavelength maxima (673 nm for Zn–BC versus 683 nm for Zn–BC–AM) due to the electron-withdrawing effect by the amidinium group.

3.2. Photocytotoxicity of Zn–BC–AM

The photocytotoxicity of Zn–BC–AM on the two NPC cell lines, namely CNE-2 and HONE-1, was determined and the results are shown in Fig. 3. In the absence of light irradiation, Zn–BC–AM was not cytotoxic to the NPC cells. A drug (0.25–2 μM) and light (0–5 J/cm^2) dose dependent cytotoxicity was observed in Zn–BC–AM sensitized CNE-2 and HONE-1 cells. At the light dose of 5 J/cm^2, the concentration of Zn–BC–AM, which causes 50% cytotoxicity on the CNE-2 and HONE-1 cells, was 1.04 and 1.24 μM, respectively. The apoptosis and the actual cell death of NPC cells as determined by the MTT assay were also confirmed by nuclear staining of apoptotic bodies and clonogenic assay (data not shown).

3.3. Subcellular localization of Zn–BC–AM

Generation of reactive oxygen species (ROS) is a general property of many photosensitizers. In a biological

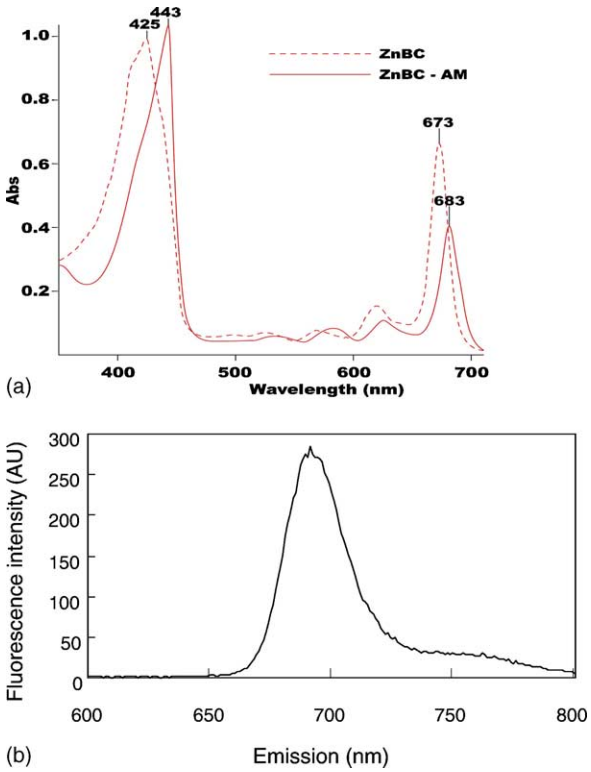

Fig. 2. Visible spectra of Zn–BC–AM. (a) Absorption characteristics of the starting material Zn–BC and the amidinium Zn–BC–AM. The spectra were recorded on a Cary 50 UV–vis spectrophotometer at 23 °C, using CH_2Cl_2 as solvent. (b) Fluorescence emission spectrum of Zn–BC–AM. The spectrum was recorded on a SLM8100 Spectrofluorimeter, using CH_2Cl_2 as solvent. AU: arbitrary units.

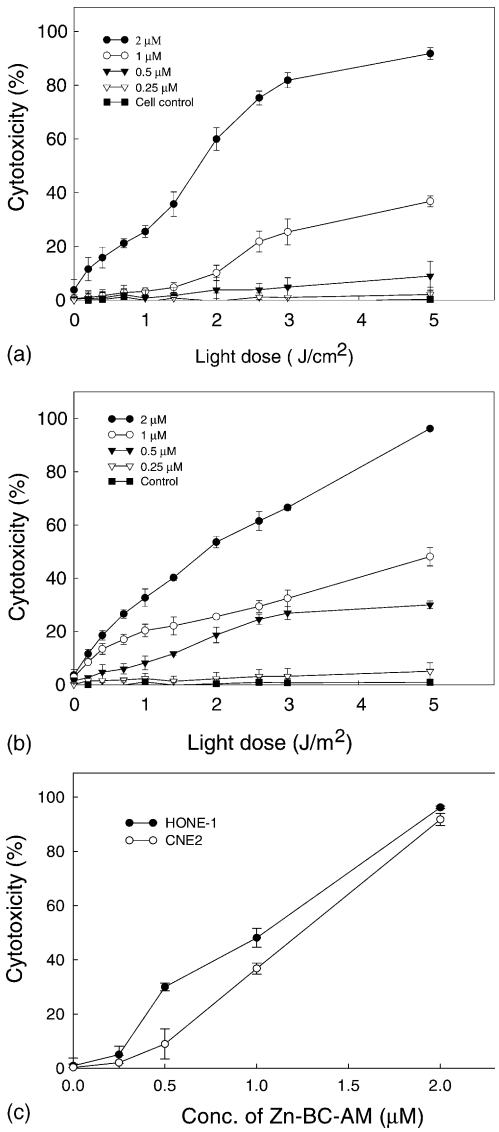

Fig. 3. Photocytotoxicity of Zn–BC–AM on NPC cells. HONE-1 (a) and CNE2 (b) cells were pre-treated with Zn–BC–AM for 24 h and then irradiated with various light doses. MTT cytotoxicity assay was carried out 24 h after PDT. The Zn–BC–AM dose–response curves of CNE-2 and HONE-1 at 5 J/cm^2 are shown in (c). Results are expressed as the mean ± S.D. of four replicates of each treatment.

environment, ROS (e.g. singlet oxygen) has a very short half-life and the migration distance is less than 0.02 μm in cells [16]. Thus, subcellular localization of the photosensitizer is usually at the site of photodamage. To investigate the subcellular localization, HONE-1 cells were co-incubated with Zn–BC–AM and organelle-specific probes. The degree of co-localization was determined by analyzing the confocal images obtained from Zn–BC–AM and the organelle probes [13,14,17]. Results in Fig. 4 show that the fluorescence signals of Zn–BC–AM overlap well with the fluorescence signals from mitochondria, ER, and Golgi body. The result suggests that Zn–BC–AM localizes mainly in these organelles of the HONE-1 cells.

3.4. Mitochondrial membrane depolarization

Mitochondria are increasingly recognized as an important target organelle during photodamage of tumour cells. In general, cell killing is preceded by a collapse of mitochondrial membrane potential $\Delta\psi_m$ and the collapse of $\Delta\psi_m$ has been implicated as a key factor to initiate a cascade of events (e.g. release of cytochrome *c* and the activation of caspases) leading to cell death [18]. We first determined the change of $\Delta\psi_m$ in Zn–BC–AM PDT-treated (2 μM, 5 J/cm^2) HONE-1 and CNE-2 cells. A leftward shift of the fluorescence curve, an indication of collapse of $\Delta\psi_m$, was seen in Zn–BC–AM PDT-treated NPC cells. Over 95% of HONE-1 and CNE-2 cells exhibit a collapse of $\Delta\psi_m$ at 15 min after light irradiation (Fig. 5b,e). The membrane remains depolarized at 1 h after irradiation (Fig. 5c,f). We next determined the release of cytochrome *c* from the mitochondria. Flow cytometric analysis was used to quantify the cells showing the release of cytochrome *c* [17]. There was a significant increase in the percentage of cytochrome *c* stained HONE-1 cells at 1 h after PDT. The percentage of HONE-1 cells showing release of cytochrome *c* at 1 and 2 h after PDT was 95.6 and 99.7%, respectively (Fig. 6).

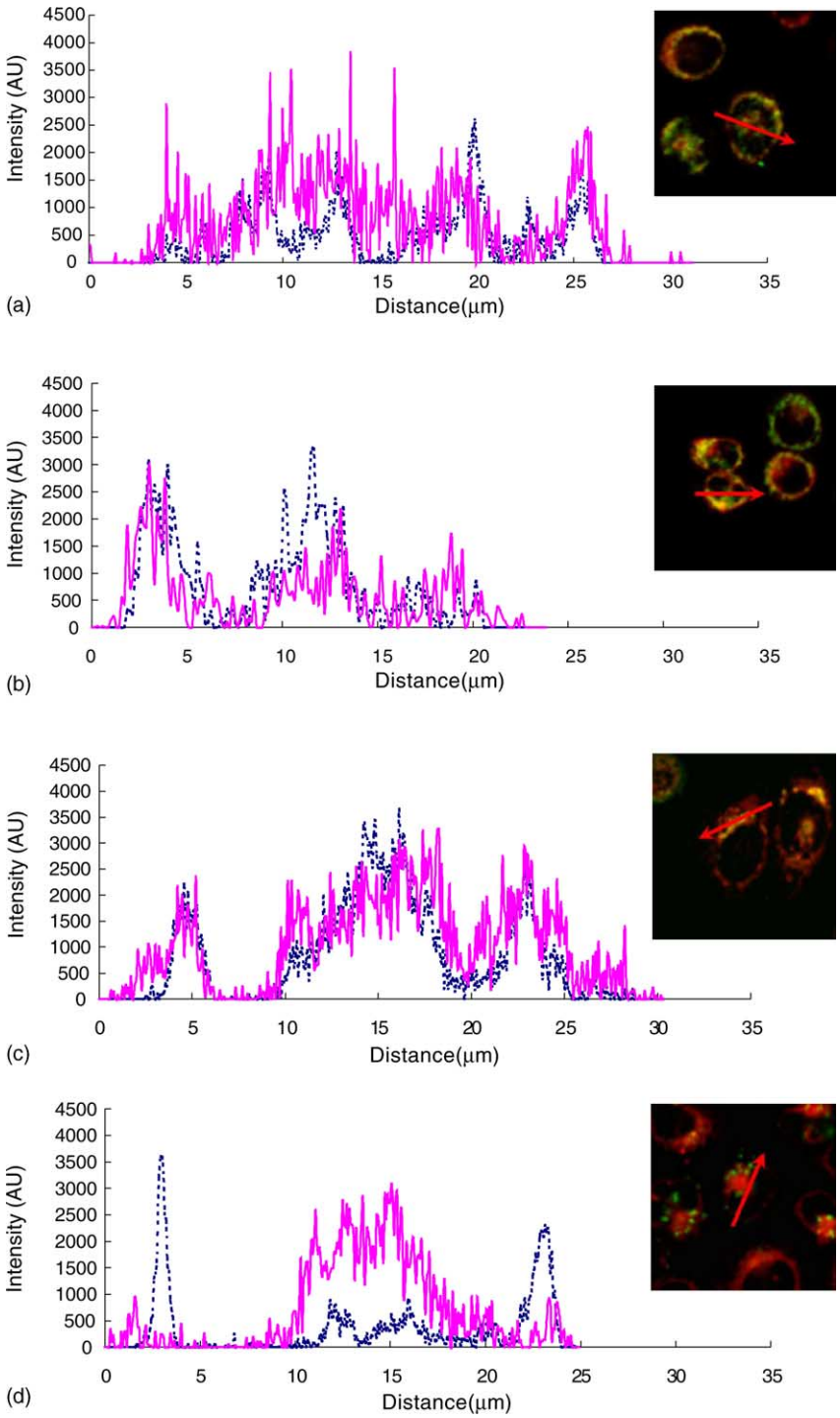

Fig. 4. Subcellular localization of Zn–BC–AM. HONE-1 cells were treated with Zn–BC–AM (2 μM) for 24 h. Cell were then stained (a) with the mitochondria probe Mito-Tracker Green FM dye M7514 (100 nM, 30 min), (b) ER probe $DiOC_6$ D273 (1 μg/ml, 1 min), (c) golgi body probe BODIPY FL C_5-ceramide D3512 (2 μM, 20 min), and (d) lysosome probe LysoTracker Green DND-26 L-7526 (250 nM, 30 min). Red dots represent the fluorescence images of Zn–BC–AM, and the green dots represent the organelle probes. The fluorescence intensity profiles of Zn–BC–AM (red lines) and the organelle probe (blue lines) are drawn along the red arrow in the confocal images.

3.5. PDT-induced ER stress

Since Zn–BC–AM localizes not only in the mitochondria, but also in the ER of the NPC cells, it is logical that photoactivation of Zn–BC–AM may also induce ER stress in Zn–BC–AM PDT-treated NPC cells. Recent studies have demonstrated a molecular link between ER-stress and the activation of apoptotic cell death. Therefore, we determined if ER resident stress proteins were activated after Zn–BC–AM PDT treatment. Western blotting was used to analyze the expression of molecular chaperone CNX, Grp78 (Bip), and Grp94. Expressions of CNX, Grp78, and Grp94 were

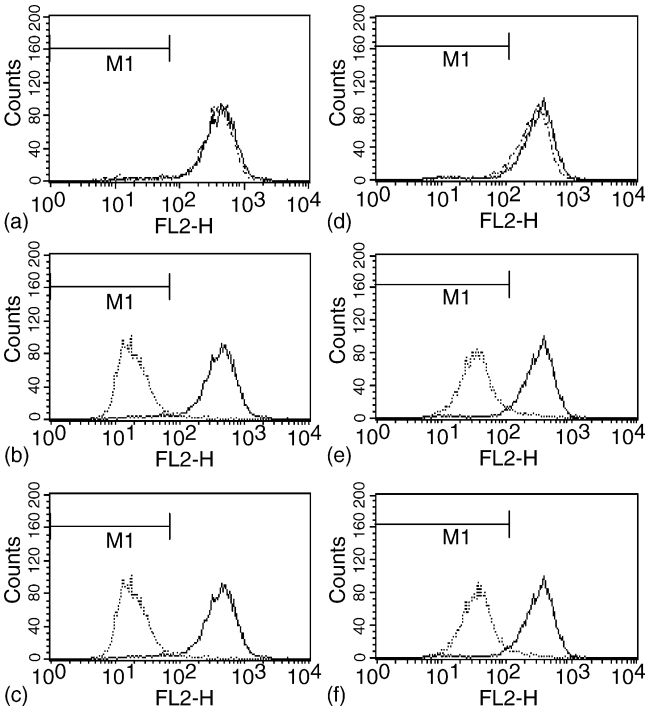

Fig. 5. Mitochondrial membrane depolarization. HONE-1 (a, b, c) and CNE-2 (d, e, f) cells were sensitized with Zn–BC–AM (2 μM) for 24 h. The cells were labeled with TMRE (150 nM) for 30 min before flow cytometric analysis. Collapse of membrane potential was determined at 15 min (b, e) and 60 min (d, f) after light illumination (5 J/cm^2). The spectral shift of the fluorescence curve (dotted line) to the left indicates mitochondrial membrane depolarization. Solid line: fluorescence signal from dark control group.

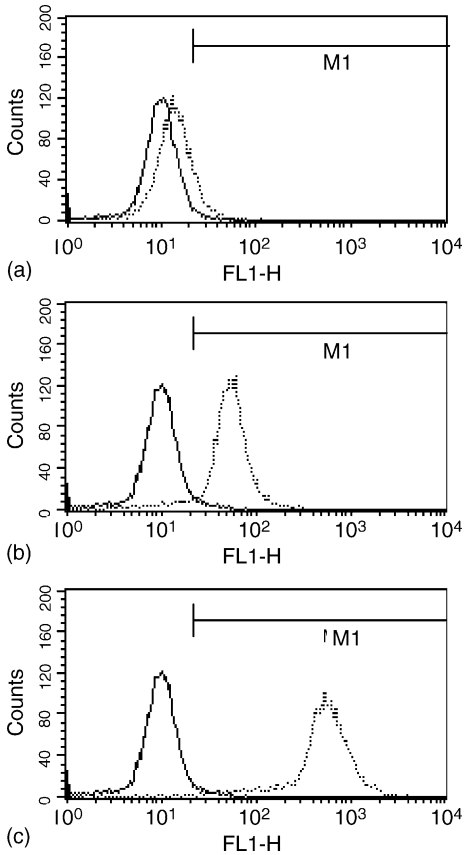

Fig. 6. Flow cytometric analysis of cytochrome *c* release in PDT-treated NPC cells. HONE-1 cells were sensitized with Zn–BC–AM (2 μM) for 24 h. PDT-treated (5 J/cm^2) NPC cells were fixed and stained with FITC-conjugated antibody at 1 h (b) or 2 h (c) after light treatment. Dark control was Zn–BC–AM sensitized HONE-1 cells (a). Solid line: dark control cell. Dotted line: PDT-treated HONE-1 cells.

up-regulated in HONE-1 cells at 2–6 h after Zn–BC–AM PDT treatment (Fig. 7). Up-regulation of expression was also observed in the CNE-2 cells (data not shown). This result prompted us to further examine the activation of a recently described apoptotic protein caspase-12. Procaspase-12 (53 kDa) is an ER resident protein and is proteolytically activated by ER stress. HONE-1 cells were PDT-treated (2 μM, 5 J/cm^2) with Zn–BC–AM and the cell lysates were subjected to Western blot analysis. A clear band of pro-caspase-12 (53 kDa as stained by Ab1 and Ab2) was observed in the immunoblot of cell lysates from untreated (cell control) and Zn–BC–AM sensitized (dark control) HONE-1 cells (Fig. 7). Activation of pro-caspase-12, as judged from the appearance of a 40 kDa (as stained by Ab-1) or 25–30 kDa (as stained by Ab-2) proteolytic fragment, was seen in Zn–BC–AM PDT-treated HONE-1 cells. The proteolytic cleavage was detected as early as 1 h after PDT. Furthermore, the expression level of pro-caspase-12 was also increased at 2–6 h after PDT. Similar results were also observed in CNE-2 cells (data not shown). These results clearly indicate that Zn–BC–AM PDT exerts ER stress on the NPC cells.

3.6. Caspase activation

Caspases are critical mediators of programmed cell death. To further establish the key caspases involved in Zn–BC–AM PDT-induced apoptosis, we measured the activities of caspase-9 and caspase-3 in PDT-treated HONE-1 cells. As shown in Fig. 8, both caspase-9 and caspase-3 were activated in Zn–BC–AM sensitized cells at 4–12 h after light irradiation. These results, together with

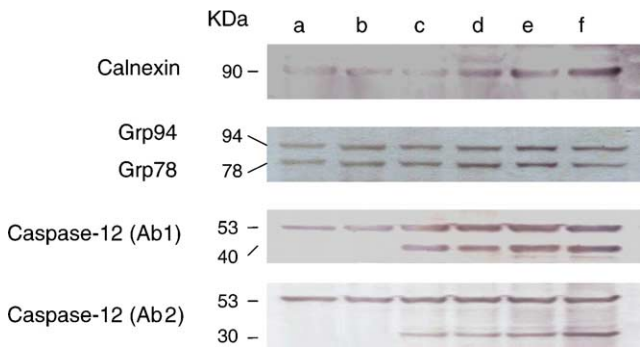

Fig. 7. Induction of ER stress. HONE-1 cells were sensitized with Zn–BC–AM (2 μM) for 24 h. The cells were then irradiated (5 J/cm^2) and cell lysates were prepared at 1–6 h after PDT. Lane (a) HONE-1 cell alone, (b) Zn–BC–AM sensitized HONE-1 cells, (c–f) Zn–BC–AM sensitized and light irradiated HONE-1 cells at 1, 2, 3 and 6 h after PDT, respectively. *Note*: anti-KDEL monoclonal antibody identifies Grp78 and Grp94 proteins.

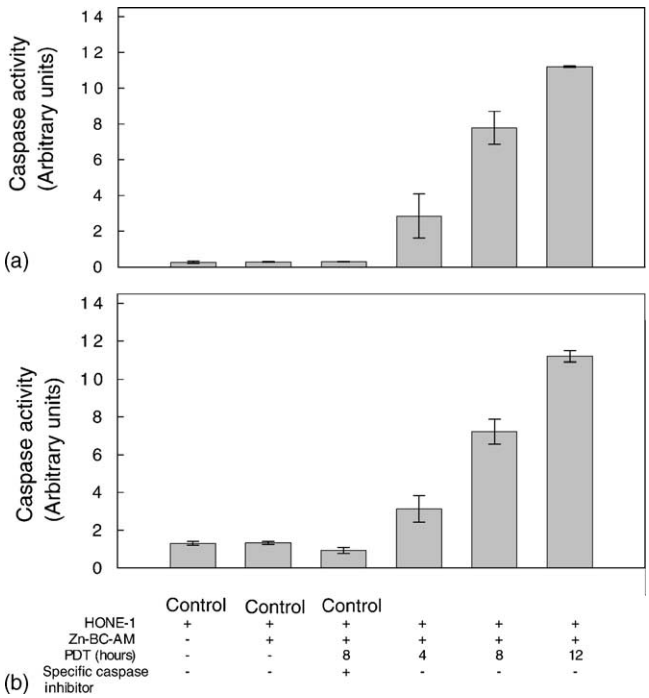

Fig. 8. HONE-1 cells were treated with Zn–BC–AM (2 μM) for 24 h. The cells were washed and exposed to 2.5 J/cm^2. The activity of caspase-9 (a) and caspase-3 (b) was determined at 4, 8, and 12 h after PDT. The specificity of the enzyme activity was verified by including the corresponding specific caspase inhibitor in the reaction mixture as suggested by the manufacturer.

the release of cytochrome *c*, indicate that mitochondria are one of the targets of photodamage during the activation of Zn–BC–AM.

3.7. Role of intracellular Ca^{2+}

The roles of Ca^{2+} in initiation of apoptotic cell death have been implicated in many studies and ER has long been known to serve as a major intracellular Ca^{2+} storage site. The ER localization of Zn–BC–AM and the induction of ER-stress during photoactivation prompted us to further investigate the role of intracellular Ca^{2+} in Zn–BC–AM PDT-induced HONE-1 cell death. Zn–BC–AM sensitized HONE-1 cells were loaded with the membrane permeable intracellular Ca^{2+} chelator EGTA–AM before PDT. Results in Table 1 show that EGTA–AM dose-dependently reduces the photocytotoxicity of Zn–BC–AM in HONE-1 cells. Efflux of Ca^{2+} from stressed-ER and the uptake of the released Ca^{2+} by mitochondria have been implicated as an important pathway leading to cell death [19]. We next examined the effect of blocking mitochondrial Ca^{2+} uptake in Zn–BC–AM PDT-induced NPC cell death. In the presence of mitochondrial Ca^{2+} uniporter inhibitor RR, the photocytotoxicity of Zn–BC–AM on HONE-1 cells was reduced from 56% in the light-irradiation group to 21% in the RR (300 μM) treatment group. Thus, the photocytotoxicity of Zn–BC–AM depends on the intracellular Ca^{2+} homestasis and Ca^{2+} uptakes by mitochondria.

Table 1
Effects of RR on Zn–BC–AM PDT treated HONE-1 cells

Zn–BC–AM	Drugs (μM)	Light treatment	Cytotoxicity (%, mean ± S.D.)
−	−	−	0.61 ± 1.02
+	−	−	0.73 ± 1.95
−	RR 200	−	0.49 ± 2.98
−	RR 300	−	0.85 ± 1.26
+	−	+	56.83 ± 2.63
+	RR 200	+	25.62 ± 3.35$^{\#}$
+	RR 300	+	21.58 ± 2.72$^{\#}$
−	−	−	0.86 ± 1.18
+	−	−	0.54 ± 1.75
−	EGTA 1	−	0.82 ± 0.91
−	EGTA 2	−	1.25 ± 2.67
+	−	+	52.69 ± 3.79
+	EGTA 1	+	38.54 ± 1.81$^{\#}$
+	EGTA 2	+	32.96 ± 2.06$^{\#}$

HONE-1 cells were incubated with Zn–BC–AM (2 μM) for 24 h. Before light treatment, HONE-1 cells were pre-treated with various concentrations of EGTA–AM (15 min) or RR (1 h) at 37 °C. The cells were then irradiated (1.7 J/cm^2), and further incubated for 24 h. Cytotoxicity was determined using the MTT cytotoxicity assay. $^{\#}$ $p < 0.05$.

4. Discussion

Recent studies reveal two distinct apoptotic mechanisms leading to cell death, namely the extrinsic cell surface receptor-mediated (e.g. tumour necrosis factor receptor) and the intrinsic mitochondria- or ER-mediated cell death pathway [20–26]. The ER stress-induced apoptotic cell death represents a novel and mitochondrial-independent intrinsic apoptotic pathway [27]. ER is essential to the functions and survival of a cell. Any perturbation of ER functions may cause cell damage and cell death. During photodynamic treatment, photosensitizers are activated and induce oxidative stress on the cells. Because of the subcellular localization of the photosensitizers and the short migration distance of singlet oxygen (less than 0.02 μm) [16], the sites of photosensitizers localization (e.g. mitochondria) have been implicated as a target in PDT-mediated apoptotic cell death of the tumor cells [14]. Although recent study has indicated the possible involvement of ER in PDT-induced apoptotic cell death, activation of the key ER resident caspase-12 was not demonstrated [28]. ER has long been known to regulate the intracellular calcium levels, protein synthesis and protein folding, and the cellular responses to stress [19,29,30]. Recent study showed that caspase-12 is localized on the membrane of ER and it is activated by ER stress such as the disruption of ER calcium homeostasis and accumulation of excess proteins in ER [21,22,31]. The activation of caspase-12 is not mediated by membrane- or mitochondrial-targeted apoptotic signals. Using a cell-free system, Rao et al. have demonstrated that the ER stress-induced apoptotic cell death represents a novel, mitochondrial and Apaf-1-independent, intrinsic apoptotic pathway [27]. However, the two organelles are not functioning independently, and there may be communication between the ER and mitochondria.

In this study, the second-generation photosensitizer Zn–BC–AM clearly triggers the mitochondria-mediated apoptotic pathway. This observation is based on the mitochondrial localization of Zn–BC–AM, induction of collapse of mitochondrial membrane potential $\Delta\psi_m$ early after light irradiation, release of cytochrome *c* and the activation of caspases-9 and -3. Since Zn–BC–AM also localizes at the ER, this observation prompted us to further examine the role of ER in Zn–BC–AM-induced NPC cell death. The expression of several ER-stress response proteins, such as CNX, Grp78 and Grp94 were increased in the NPC cells after Zn–BC–AM PDT. CNX, a membrane protein localized in the ER, has been shown to play a key role in glycoprotein folding and quality control within the ER by interacting with folding intermediates via their monoglucosylated glycans [32]. In ER stress-induced apoptotic cells, CNX appears to be involved in later events by forming complexes with the pro-apoptotic caspase-8 substrate Bap31. Furthermore, cells with CNX-deficiency were more resistant than normal cells to apoptosis induced by ER stress [26]. In this study, the expression of CNX was significantly increased at about 2 h after photoactivation. The expression was maintained at a high level between 2 and 6 h after PDT. Taken together, CNX might play a role in a later event of Zn–BC–AM PDT induced apoptosis.

Normal cells respond to ER-stress by increasing transcription of genes encoding ER-resident chaperones such as the glucose-regulated proteins Grp78/BiP and Grp94. Induction of these molecular chaperones helps to control intracellular Ca^{2+} homeostasis and prevents toxicant-induced cell death. Grp94 is a representative ER-stress-induced protein of the Hsp90 family. It is a glycoprotein resident in the lumen of ER and is responsible for Ca^{2+} binding and scavenging of the unfolded proteins. Although Grp94 can protect cells from oxidative damage, apoptotsis can still occur if stress in the tissue is too strong [26,33]. Grp78 is an ER-resident protein and it is thought to be involved in regulation of cell death under ER stress. In addition to the regulation of intracellular Ca^{2+}, Grp78 has also been considered as an anti-apoptotic regulatory molecule [34]. Earlier studies showed that ER stress induced the formation of Grp78-procaspase-12-procaspase-7 complex [24]. This will prevent the proteolytic cleavage of procaspases. However, cellular insult that causes prolonged ER stress can result in the disruption of the Grp78-procaspase-12-procaspase-7 complex. The release of activated caspase-12 may then activate caspase-9 and lead to apoptotic cell death [23,24,27]. In this study, Zn–BC–AM PDT may cause a prolonged ER stress, as judged from the continuous expression of the molecular chaperones such as Grp94 and CNX, on the NPC cells. Furthermore, caspase-12 activation was also detected in the first few hours after Zn–BC–AM PDT. These results indicated that Zn–BC–AM PDT induced ER-stress also play a role in apoptotic cell death of NPC cells.

Both the mitochondria and ER are important in controlling apoptotic cell death. Treating of NPC cells with Zn–BC–AM results in the subcellular localization of this sensitizer in mitochondria and ER. To further establish the temporal relationship between the ER and mitochondrial localization of Zn–BC–AM and the cell death in NPC cells, we examined the blocking effect of two inhibitors RR and EGTA–AM on Zn–BC–AM PDT treated NPC cells. These 2 inhibitors had previously been shown to block Ca^{2+} uptake by mitochondria and buffer Ca^{2+} release from ER [19]. Our data show that Zn–BC–AM induced cytotoxicity was sensitive to intracellular Ca^{2+} chelator EGTA–AM and the inhibitor of Ca^{2+} uptake in the mitochondria (RR). Since ER is known to be the major intracellular Ca^{2+} store, it is logical that PDT-induced ER-stress may result in Ca^{2+} release from the ER and confer cell sensitivity to mitochondria-mediated apoptotic cell death. In conclusion, our data support the model of ER-mitochondria cross-talk in which both mitochondria and ER-mediated apoptotic pathways are involved in Zn–BC–AM PDT induced NPC cell death. Zn–BC–AM appears to be a candidate photosensitizer for the photodynamic treatment of NPC.

Acknowledgement

This work was supported by the Research Grants Council of Hong Kong (Project nos. CA99/00SC2 and HKBU 2052/02M).

References

[1] Mould RF, Tai TH. Nasopharyngeal carcinoma: treatments and outcomes in the 20th century. Br J Radiol 2002;75:307–39.
[2] Ibbotson SH. Topical 5-aminolaevulinic acid photodynamic therapy for the treatment of skin conditions other than non-melanoma skin cancer. Br J Dermatol 2002;146:178–88.
[3] McCaughan Jr JS. Photodynamic therapy: a review. Drugs Aging 1999;15:49–68.
[4] Ackroyd R, Kelty C, Brown N, Reed M. The history of photodetection and photodynamic therapy. Photochem Photobiol 2001;74:656–69.
[5] Piette J, Volanti C, Vantieghem A, Matroule JY, Habraken Y, Agostinis P. Cell death and growth arrest in response to photodynamic therapy with membrane-bound photosensitizers. Biochem Pharmacol 2003;66:1651–719.
[6] Graham A, Li G, Chen Y, Morgan J, Oseroff A, Dougherty TJ, et al. Structure-activity relationship of new octaethylporphyrin-based benzochlorins as photosensitizers for photodynamic therapy. Photochem Photobiol 2003;77:561–6.
[7] Morgan J, Whitaker JE, Oseroff AR. GRP78 induction by calcium ionophore potentiates photodynamic therapy using the mitochondrial targeting dye Victoria Blue BO. Photochem Photobiol 1998;67:155–64.
[8] Hsieh YJ, Wu CC, Chang CJ, Yu JS. Subcellular localization of Photofrin determines the death phenotype of human epidermoid carcinoma A431 cells triggered by photodynamic therapy: when plasma membranes are the main targets. J Cell Physiol 2003;194.
[9] Oleinick NL, Evans HH. The photobiology of photodynamic therapy: cellular targets and mechanisms. Radiat Res 1998;150:S146–56.

[10] Oleinick NL, Morris RL, Belichenko I. The role of apoptosis in response to photodynamic therapy: what, where, why, and how. Photochem Photobiol Sci 2002;1:1–21.
[11] Daniel PT. Dissecting the pathways to death. Leukemia 2000;14:2035–44.
[12] Hendrickx N, Volanti C, Moens U, Seternes OM, de Witte P, Vandenheede JR, et al. Up-regulation of cyclooxygenase-2 and apoptosis resistance by p38 MAPK in hypericin-mediated photodynamic therapy of human cancer cells. J Biol Chem 2003;278:52231–9.
[13] Mak NK, Kok TW, Wong RN, Lam SW, Lau YK, Leung WN, et al. Photodynamic activities of sulfonamide derivatives of porphycene on nasopharyngeal carcinoma cells. J Biomed Sci 2003;418–29.
[14] Chen JY, Cheung NH, Fung MC, Wen JM, Leung WN, Mak NK. Subcellular localization of merocyanine 540 (MC540) and induction of apoptosis in murine myeloid leukemia cells. Photochem Photobiol 2000;114–20.
[15] Bai G, Rama Rao KV, Murthy CR, Panickar KS, Jayakumar AR, Norenberg MD. Ammonia induces the mitochondrial permeability transition in primary cultures of rat astrocytes. J Neurosci Res 2001;66:981–91.
[16] Moan J, Berg K. The photodegradation of porphyrins in cells can be used to estimate the lifetime of singlet oxygen. Photochem Photobiol 1991;53:549–53.
[17] Chen JY, Mak NK, Yow CM, Fung MC, Chiu LC, Leung WN, et al. The binding characteristics and intracellular localization of temoporfin (mTHPC) in myeloid leukemia cells: phototoxicity and mitochondrial damage. Photochem Photobiol 2000;72:541–57.
[18] Lemasters JJ, Nieminen AL, Qian T, Trost LC, Elmore SP, Nishimura Y, et al. The mitochondrial permeability transition in cell death: a common mechanism in necrosis, apoptosis and autophagy. Biochim Biophys Acta 1998;1366:177–96.
[19] Liu H, Bowes III RC, van de WB, Sillence C, Nagelkerke JF, Stevens JL. Endoplasmic reticulum chaperones GRP78 and calreticulin prevent oxidative stress, Ca^{2+} disturbances, and cell death in renal epithelial cells. J Biol Chem 1997;272:21751–9.
[20] Schulze-Osthoff K, Ferrari D, Los M, Wesselborg S, Peter ME. Apoptosis signaling by death receptors. Eur J Biochem 1998;254:439–59.
[21] Nakagawa T, Zhu H, Morishima N, Li E, Xu J, Yankner BA, et al. Caspase-12 mediates endoplasmic-reticulum-specific apoptosis and cytotoxicity by amyloid-beta. Nature 2000;403:98–103.
[22] Nakamura K, Bossy-Wetzel E, Burns K, Fadel MP, Lozyk M, Goping IS, et al. Changes in endoplasmic reticulum luminal environment affect cell sensitivity to apoptosis. J Cell Biol 2000;150:731–40.
[23] Rao RV, Hermel E, Castro-Obregon S, del Rio G, Ellerby LM, Ellerby HM, et al. Coupling endoplasmic reticulum stress to the cell death program Mechanism of caspase activation. J Biol Chem 2001;276:33869–74.
[24] Rao RV, Peel A, Logvinova A, del Rio G, Hermel E, Yokota T, et al. Coupling endoplasmic reticulum stress to the cell death program: role of the ER chaperone GRP78. FEBS Lett 2002;514:122–8.
[25] Xie Q, Khaoustov VI, Chung CC, Sohn J, Krishnan B, Lewis DE, et al. Effect of tauroursodeoxycholic acid on endoplasmic reticulum stress-induced caspase-12 activation. Hepatology 2002;36:592–601.
[26] Zuppini A, Groenendyk J, Cormack LA, Shore G, Opas M, Bleackley RC, et al. Calnexin deficiency and endoplasmic reticulum stress-induced apoptosis. Biochemistry 2002;41:2850–8.
[27] Rao RV, Castro-Obregon S, Frankowski H, Schuler M, Stoka V, del Rio G, et al. Coupling endoplasmic reticulum stress to the cell death program An Apaf-1-independent intrinsic pathway. J Biol Chem 2002;277:21836–42.
[28] Grebenova D, Kuzelova K, Smetana K, Pluskalova M, Cajthamlova H, Marinov I, et al. Mitochondrial and endoplasmic reticulum stress-induced apoptotic pathways are activated by 5-aminolevulinic acid-based photodynamic therapy in HL60 leukemia cells. J Photochem Photobiol B 2003;69:71–85.
[29] Liu H, Miller E, van de WB, Stevens JL. Endoplasmic reticulum stress proteins block oxidant-induced Ca^{2+} increases and cell death. J Biol Chem 1998;273:12858–62.
[30] Rapoport TA. Transport of proteins across the endoplasmic reticulum membrane. Science 1992;258:931–6.
[31] Oyadomari S, Araki E, Mori M. Endoplasmic reticulum stress-mediated apoptosis in pancreatic β-cells. Apoptosis 2002;7:335–45.
[32] Denzel A, Molinari M, Trigueros C, Martin JE, Velmurgan S, Brown S, et al. Early postnatal death and motor disorders in mice congenitally deficient in calnexin expression. Mol Cell Biol 2002;22:7398–404.
[33] Chen X, Ding Y, Liu CG, Mikhail S, Yang CS. Overexpression of glucose-regulated protein 94 (Grp94) in esophageal adenocarcinomas of a rat surgical model and humans. Carcinogenesis 2002;23:123–30.
[34] Kaufman RJ. Stress signaling from the lumen of the endoplasmic reticulum: coordination of gene transcriptional and translational controls. Genes Dev 1999;13:1211–33.